Research Square

Preprints are preliminary reports that have not undergone peer review.
They should not be considered conclusive, used to inform clinical practice,
or referenced by the media as validated information.

Intermanual transfer of a de novo motor skill relates to intrinsic sensorimotor network organization

Yonghyun Kwon
Hanyang University
Caraballo Antoine
Hanyang University
Seulgi Eun
Korea Institute of Oriental Medicine
Sungshin Kim
sungshinkim@hanyang.ac.kr

Hanyang University

Article

Keywords: Intermanual transfer, de novo motor learning, fMRI, resting-state functional connectivity, supplementary motor area (SMA), parietal cortex

Posted Date: September 15th, 2026

DOI: https://doi.org/10.21203/rs.3.rs-10650672/v1

License: This work is licensed under a Creative Commons Attribution 4.0 International License.
Read Full License

Additional Declarations: No competing interests reported.

Intermanual transfer of a de novo motor skill relates to intrinsic sensorimotor network organization

Authors: Yonghyun Kwon[1,7], Caraballo Antoine[1,7], Seulgi Eun[2,3], Sungshin Kim[1,4,5,6]*

1. Department of Data Science, Hanyang University, 04763 Seoul, Republic of Korea
2. KM Science Research Division, Korea Institute of Oriental Medicine, 34054 Daejeon, Republic of Korea
3. NeuroGlymph Imaging and Modulation Center, Korea Institute of Oriental Medicine, 34054 Daejeon, Republic of Korea
4. Department of Artificial Intelligence, Hanyang University, 04763 Seoul, Republic of Korea
5. Department of Healthcare Digital Engineering, Hanyang University, 04763 Seoul, Republic of Korea
6. Center for Neuroscience Imaging Research, Institute for Basic Science, Suwon 16419, Republic of Korea
7. These two authors equally contributed to this study

*Corresponding Author
222 Wangsimni-ro Seongdong-gu, Seoul, Republic of Korea
Email: sungshinkim@hanyang.ac.kr
Phone: +82-10-4687-5322

Abstract

Intermanual transfer refers to the improvement in performance of an untrained hand after practice with the opposite hand, reflecting shared neural representations of motor skills across the two cerebral hemispheres. Previous studies on motor learning transfer have produced inconsistent findings, largely due to differences in task characteristics, such as adaptation or sequence learning paradigms. Notably, intermanual transfer has not been systematically explored during *de novo* motor skill acquisition. In the present study, participants learned a *de novo* motor task with one initial hand and subsequently performed the same task with the opposite hand. Although the initial learning of both hands did not differ, transfer effects were asymmetric: greater performance gains were observed when participants practiced initially with their non-dominant hand and then switched to the dominant hand, compared to the reverse order. Furthermore, intrinsic functional organization of the sensorimotor network assessed by resting-state functional connectivity accounted for individual differences in the extent of the intermanual transfer across participants, regardless of hand order. These findings suggest that intermanual transfer during *de novo* motor skill learning is asymmetric and associated with the functional interaction among regions within sensorimotor network, providing mechanistic insights for bilateral motor rehabilitation strategies.

Keywords: Intermanual transfer, *de novo* motor learning, fMRI, resting-state functional connectivity, supplementary motor area (SMA), parietal cortex

Introduction

Humans continually learn new motor skills in their everyday lives, and one remarkable feature of that learning is its transferability, which allows individuals to apply motor skills learned in one context to novel environments, or different body parts [1]. One manifestation of this generalization is intermanual transfer – the phenomenon where training one hand leads to performance gains in the opposite. This transfer suggests that motor learning is not merely effector-specific but is supported by neural representations that are shared and coordinated across cerebral hemispheres [2].

Behavioral studies have shown that the extent and direction of intermanual transfer are modulated by various factors. Transfer is often asymmetric, with more effective transfer from the dominant to the non-dominant hand [3,4]. However, symmetrical transfer has been shown to emerge in the early stages of motor learning, when the cognitive mechanisms underlying the learning strategy are equally applicable to both hands [5]. Moreover, the asymmetry in intermanual transfer varied with task complexity, with transfer particularly facilitated in complex tasks that placed greater cognitive demands than simple tasks [6]. Even after successfully learning a complex task with one hand, transferability becomes highly limited when the motor context changes, such as when a skill must be performed bimanually rather than unimanually [7, 8].

Neuroimaging and neurophysiological research have identified a distributed motor network, supporting intermanual transfer, including the primary motor cortex (M1), supplementary motor area (SMA), parietal regions, subcortical motor circuits, and interhemispheric callosal pathways [2, 9]. Within this network, SMA plays a central role in mediating the coordination and integration of bilateral motor activity, enabling efficient transfer across effectors, while the cerebellum and striatal-thalamic-cortical pathways contribute more to the early stages of learning [10-12]. For example, Perez et al. linked intermanual transfer of a newly acquired finger sequence to an SMA-thalamic circuit, with SMA and ventrolateral thalamic activity associated with transfer-related performance [2]. A subsequent TMS study further provides causal evidence regarding contribution of the SMA to intermanual transfer [13].

However, more recent work has investigated larger-scale network interactions, including higher-order cognitive and attentional processes. Evidence indicates that dynamic cross-hemispheric interactions, modulated by the level of interhemispheric inhibition, shape the transfer [14]. Intrinsic hippocampus-ventromedial prefrontal cortex (vmPFC) connectivity is also implicated in the generalization of learned skills [15]. Lastly, interaction between attentional and executive control networks suggest that neural resources allocation is critical for the transfer process [16].

Clarifying what information is transferred during the transfer process is also needed. Effector-independent learning (learning that is not specific to a particular body part), appears to facilitate cross-limb transfer by encoding motor representations in both extrinsic and intrinsic reference frames [17]. This result is consistent with evidence that intermanual transfer is mediated by higher-order neural mechanisms beyond simple motor control. Converging evidence further indicates that striatal-thalamic-cortical pathways play an important role in the early stages of learning, whereas cerebellar-motor cortical interactions contribute more as learning stabilizes and transfers across hemispheres [11]. Other studies showing that the left posterior parietal cortex (PPC) facilitates effector-independent motor memory suggests that intermanual transfer may not simply depend on a specific effector but may be mediated by higher-level cognitive integration

mechanisms [18]. Taken together, successful intermanual transfer may depend on the intrinsic organization of a shared sensorimotor network that supports visuomotor mapping, sensory feedback processing, motor planning, and cross-effector coordination.

Despite these advances, most evidence on intermanual transfer derives from motor sequence learning or sensorimotor adaptation, or relatively simple motor tasks. Far less is known about the extent and neural mechanisms of intermanual transfer in *de novo* skill learning, in which individuals construct an entirely new sensorimotor mapping rather than recalibrate an existing one or repeat a predefined sequence [19-23].

In our previous work, we designed a *de novo* learning task, in which participants learned to control a cursor using their finger movement [24]. In the task, participants must learn and stabilize a mapping between high-dimensional finger movements and two-dimensional cursor movements. Such learning requires extensive exploration, feedback-based control, visuomotor integration, and motor planning, making it especially suitable for examining how newly acquired motor skill generalizes across hands.Another important question is why the extent of intermanual transfer varies across individuals. Previous studies have linked individual differences in transfer to task-evoked activity and network coupling during training [2, 25-27], the neural basis of individual variability remains less understood, particularly during of *de novo* motor learning. Such variability may reflect the intrinsic functional organization of a shared sensorimotor network across effectors, consistent with evidence that baseline resting-state functional connectivity predicts individual differences in motor learning [28-30].

Thus, the present study explores how transfer between the dominant and non-dominant hand emerges when learning our *de novo* cursor-control task and examines whether individual differences in transfer are associated with the intrinsic organization of a shared sensorimotor network. Our study of intermanual transfer in de *novo* skill learning bridges the gap between the adaptive neuroplasticity observed in simple motor tasks and the sophisticated skill acquisition required in real-world situations. Understanding how individual variability in intrinsic sensorimotor network organization shapes intermanual transfer may also provide a foundation for designing individualized rehabilitation strategies that use training of the less-affected hand to promote motor recovery and skill transfer to the affected hand [31-33].

Methods

Participants

The study enrolled 38 individuals, of whom 32 participants (16 female, mean age ± SD = 23.9 ± 2.1 years, age range = 21-28 years) had no history of neurological or psychiatric disorders and completed both functional magnetic resonance imaging (fMRI) and behavior sessions. All participants were right-handed, as assessed by the modified Edinburgh Handedness Inventory [34]. Prior to the first experiment, all participants provided written informed consent and received monetary compensation for their participation. The Institutional Review Board (IRB) of Sungkyunkwan University, Suwon, South Korea approved all procedures related to the study following safety protocols (IRB No. 2018-05-003-032). We performed all the research methods in accordance with the Declaration of Helsinki.

Experimental procedures

Day 1: fMRI session

During the first visit, participants completed one run of a 9-min-long resting-state fMRI (rs-fMRI) followed by a localizer task, both inside the MRI scanner. For the resting-state run, participants were instructed to keep their eyes open, fixated on a crosshair in the center of the screen, and

tried not to engage in specific thoughts. The localizer task was performed to define brain regions related to random finger movements. Participants performed a cued hand-movement task while wearing MR-compatible gloves (5DT Glove 14 Ultra) that recorded finger joint movements in real time. Two gray squares appeared side-by-side on the screen and when the squares turned red, participants moved the corresponding hand. The localizer task comprised 18 movement trials (15s each) interleaved with 15s rest, performed sequentially to the left hand, the right hand, and finally both hands (Figure 1A. fMRI experiment).

Day 2: Behavioral training session

Familiarization and calibration. For the second visit, participants first familiarized themselves with the MR-compatible data glove on their dominant right hand by freely moving their fingers while observing 13 onscreen connected dots that moved in real-time, each corresponding to a specific glove sensor (Figure 1B. Behavior experiment). Participants were instructed to explore different hand postures and movements, and 13 of the 14 sensors on each data glove were used to record movements. The last malfunctioning sensor was removed from further analysis for all participants. They then performed a similar calibration of the glove with both hands to establish the hand-cursor mapping. The mapping between the hand and the cursor was defined as follows [24, 25].

$$[x\ y\ ] = \left[a_{x,1}\ a_{x,2}\ \dots\ a_{x,12}\ a_{x,13}\ a_{y,1}\ a_{y,2}\ \dots\ a_{y,12}\ a_{y,13}\ \right] \times [h_1\ h_2\ \dots\ h_{12}\ h_{13}\ ]^T + \left[x_0\ y_0\ \right],$$

where $h_k(k = 1, 2, \dots, 13)$ is the vector of finger movement obtained from the 13 sensors of the data glove, and x and y denote the horizontal and vertical positions of the cursor. The time series data from the 13 sensors were sampled at 60 Hz, and the resulting covariance matrix was used to perform a principal component analysis, where $p = Ah + p_0$ and the mapping matrix A was generated by mapping the first two principal components to the horizontal (x) and vertical (y) cursor axes, while the offset p_0 centered the cursor. As a result, finger movement was recorded by 13 sensors and translated into cursor positions on a two-dimensional screen through the predetermined mapping between cursor and finger movements. While the PCA-based hand-to-cursor mapping inherently captures the natural kinematic of the hand, the translation of these high-dimensional coordination patterns into a 2D screen is arbitrary. Because participants possess no prior internal model dictating how these specific finger joint configurations drive the cursor, the task cannot be solved through an error-driven learning mechanism of an existing control policy. Instead, participants must build a new controller, distinguishing this paradigm as *de novo* motor learning rather than adaptation. To verify this mapping without providing additional practice, participants faced away from the screen while the experimenter confirmed that the hidden cursor could reach every cell of a 5 × 5 grid. Calibration ended only after all 25 cells were reliably accessible for the participant.

***De novo* intermanual transfer task.** Immediately after the calibration task, participants performed the *de novo* motor skill learning task described in our previous study [24] in a separate room outside of the MRI. Participants learned to move a cursor to reach a target displayed for 5 s in one of the four corner cells of a 5 x 5 grid using finger movement. The *de novo* task comprised two phases: the training and transfer phase. Each phase included six behavioral runs, with one

run consisting of 8 blocks of 13 target tracking movements, for a total of 104 tracking movements within a run. Each run was separated by approximately a 1-minute break. The participants were required to place the cursor on the target as quickly and accurately as possible and maintain the cursor on the target. The sequence of targets was repeated in the following order: 13 (center)-1 (top left)-21 (bottom left)-25 (bottom right)-5 (top right)-1-25-21-5-25-1-5-21-1. Setting targets at extreme locations, such as the corners, encourages participants to explore the full range of 13-dimensional finger joint movements to their limits. If the targets were clustered in the center or distributed randomly, participants could complete the task with only subtle, localized movements, making it difficult to verify whether they had fully learned the mapping. The first target of each block was fixed at position 13 (center) to initialize the cursor's position on the screen. Thus, the first target tracking movement of each block was excluded from further analysis. Participants were randomly assigned to two groups: the Right-to-Left (RL) group and the Left-to-Right (LR) group, ensuring that both groups had similar distributions of gender and age. In the RL group, participants used their right hand for the training phase and their left hand during the transfer phase. Conversely, participants in the LR group used their left hand for the training phase and their right hand during the transfer phase. All visual stimuli presented to participants in the experiment and the recording of movement data through the data glove were performed using Psychtoolbox-3 in MATLAB R2021b.

MRI data acquisition

We collected fMRI data using a 3T Siemens MAGNETOM Prisma scanner with a 64-channel head coil. Functional images were obtained using an accelerated 2D gradient-echo echo-planar imaging (GE-EPI) sequence: echo time/repetition time (TE/TR) = 27.2/460 ms; flip angle (FA) = 44°; field of view (FOV) = 220 mm; matrix size = 82 × 82 ; slice thickness = 2.7 mm ; 56axial slices; slice acceleration factor = 8; 1096 dynamics (resting-state) or 1200 dynamics (motor task). To enable subsequent distortion correction, we conducted a short scan to acquire two functional volumes with opposite phase encoding directions (i.e., anterior to posterior and posterior to anterior) right before the resting state functional run. As an anatomical reference, a T1-weighted anatomical scan using MPRAGE sequence was conducted: TE/TR = 2.34/2400 ms; inversion time = 1150 ms; FA = 8°; FOV = 224 mm; matrix size = 320 × 320; slice thickness = 0.7 mm; 224 sagittal slices.

fMRI data preprocessing

The T1 and fMRI data were preprocessed following a standard procedure suggested by Analysis of Functional NeuroImages (AFNI) software [35, 36]. The inhomogeneity in the T1 image due to magnetic field bias was corrected, and the skull was removed using AFNI's "3dUnifize" and "3dSkullStrip", respectively. The preprocessing removed abnormally high signals (spikes) from the time series data ('3dDespike') and synchronized the time of the data by correcting the slice timing ('3dTshift'). The data were then distortion corrected based on the calculated fieldmap using two functional images with opposite phase encoding directions('3dQwarp') and motion corrected by aligning each volume to a reference volume ('3dvolreg'). The corrected data was spatially aligned and normalized by aligning the EPI data with the anatomical data and then aligned to the Montreal Neurological Institute 152 (MNI152) template ('align_epi_anat' 'auto_warp') and resampled to 2.7 mm isometric voxels. They were then spatially smoothed with a 4 mm Full Width

at Half Max (FWHM) Gaussian kernel to improve the spatial signal-to-noise ratio (SNR) ('3dmerge'), and each time series data was scaled from 0 to 200 with an average value of 100 to maintain consistency in signal intensity ('3dcalc'). For resting-state functional connectivity analysis, residual time series were generated by performing nuisance regression and censoring ('3dTproject'). Motion-related nuisance regressors were included through the regression matrix, and local white matter signals were regressed out using AFNI's ANATICOR approach with a '-dsort' option ('Local_FSWe_rall'). Censored time points were handled during the projection step, and the resulting residual time series were used for functional connectivity estimation. Finally, all data quality was checked using the afni_proc.py quality control (APQC) document [37].

ROI definition

Regions of interest (ROIs) were defined using the localizer functional data. A subject-level general linear model was used to estimate the blood-oxygen-level-dependent (BOLD). Left-hand, right-hand, and both-hand movements were modeled separately as distinct regressors of interest. Each trial was modeled as a boxcar function then convolved with the canonical hemodynamic response. Six motion parameters (three displacements and three rotations) as well as a polynomial regressor to account for low-frequency components were included as regressors. From this model, linear contrasts were computed to compare BOLD changes during the left-hand, right-hand, and both-hand finger movement, resulting in three separate activation maps for each subject. These individual results were then used in a group-level one-sample t-test to generate group-averaged activation maps. To define the network of brain regions commonly engaged during both left-hand and right-hand movements, we first thresholded the group-level activation maps for the unimanual left-hand and right-hand conditions using an uncorrected voxel-wise threshold of $p < 0.001$, and further thresholded by a cluster-level corrected $p < 0.05$ ('3dttest++'). We then performed a conjunction analysis between the thresholded left-hand and right-hand maps to define the overlapping regions commonly engaged during finger movements. To restrict these functional clusters to precise structural boundaries, we intersected the group-level conjunction map (left-hand AND right-hand movement) with the anatomical regions defined by the Brainnetome atlas [38] and SUIT atlas for the cerebellum [39]. Finally, we defined a sphere of 5mm (27 voxels) around the highest functional activation point (peak *t*-value averaged for right-hand and left-hand conditions) within the boundaries of the intersected atlas regions. We defined in total 15 regions (Figure 3; Table S1 for the coordinates) including the bilateral inferior parietal lobule (IPL), bilateral intraparietal sulcus (IPS), bilateral cerebellum lobule VI and VIII (CB6 and CB8), SMA, bilateral putamen and bilateral dorsal (PMd) and ventral premotor cortex (PMv).

Behavioral data analysis

In the behavioral experiment of *de novo* motor-learning task, the individuals' learning performance was assessed by how long participants could keep a target red (i.e., hitting a target with the cursor) (Figure 1B). In a block of 14 targets, excluding the time for the first target to appear to initialize the cursor position, the learning performance was calculated as the time the target remained red for the 5 seconds, as in the equation below:

$$Performance = \left\langle \frac{Time\ Target\ Remained\ Red}{Total\ Time\ of\ a\ Trial} \right\rangle_{block}$$

To maximize the performance, participants were required to navigate to the target as quickly as possible and maintain the cursor on the target. Thus, a higher performance on an individual trial reflects rapid, accurate motor movement, while sustained performance across multiple trials indicates successful de *novo* learning of the hand-to-cursor mapping. As such, a participant's performance was calculated by averaging the tracking scores within each block. Each participant performed 48 blocks, for a total of 672 target tracking movements per training and transfer phase.

To characterize individual learning, we fit an exponential growth model to each participant's block-wise performance for each phase, $f(x) = a \cdot (1 - e^{-b \cdot x}) + c$. Then, to determine whether participants attained a performance plateau during the initial 48-block training phase, we established a mathematical threshold based on the parameters of their individualized exponential curve fits. Specifically, the onset of the plateau was defined as the point at which the exponential component of the model fell to 1% of its initial value ($e^{-bx} = 0.01$). The specific block index (x) at which this occurred was calculated as $x = -ln(0.01)/b$,where b represents the individual's exponential rate constant (the dynamic rate of performance improvement). Participants whose calculated plateau onset occurred prior to the conclusion of the training phase ($x < 48$) were classified as having reached a stable execution ceiling. For these individuals, the duration of the plateau was quantified as the total number of training blocks remaining after this threshold was crossed.

To identify between groups differences, a linear mixed-effects model was used to predict the performance between the RL and LR groups in the following form:

$$Performance \sim Block * Group * Phase + (1|Participant)$$

Where Block represents the block number from 1 to 48, Group corresponds to either the RL or LR group, Phase corresponds to either the training phase or the transfer phase, and (1|Participant) reflects the random intercept assigned to each participant.
The transfer rate for each participant was defined as follows:

$$Transfer\ rate = \frac{Transfer\ of\ initial\ performance}{Total\ performance\ improvement\ during\ training}$$

The transfer of initial performance was defined as the average performance of the first eight blocks of the transfer phase (104 trials in total) minus that of the training phase. The total performance improvement during training was defined as the average performance of the last eight blocks of the training phase minus that of the training phase. Thus, the transfer rate reflects the magnitude of the initial performance that was transferred upon switching hands, relative to the performance improvement achieved by each participant during the training phase.

Resting-state functional connectivity analysis

For each of the 15 seed regions, the mean blood-oxygen-level-dependent (BOLD) signal time course was extracted from the participant's preprocessed residual resting-state data using 5mm

spherical masks. Functional connectivity between all region pairs was estimated by computing Pearson correlation coefficients (*r*) between their respective time series, yielding a comprehensive, symmetrical ROI-to-ROI correlation matrix for each subject. All raw *r*-values were converted to *z*-scores utilizing a Fisher *z*-transformation prior to further statistical analysis.

Brain-behavior correlation mapping

To investigate the neural mechanisms underlying intermanual transfer, we conducted a comprehensive whole-network brain-behavior correlation analysis. Notably, to isolate individual variability and account for baseline differences between the right-to-left and left-to-right transfer directions (as all participants are right-handed), the transfer rate should be normalized within each of RL and LR groups. The normalized intermanual transfer rate for each subject served as the primary behavioral metric. The Fisher z-transformed functional connectivity strength of all unique edges within the 15-node network (105 independent connections) was correlated with the intermanual transfer rate. While the SMAwas of primary theoretical interest given its established role in interhemispheric coordination, the whole-network approach allowed for an unbiased identification of the pathways associated with intermanual transfer. To control for multiple comparisons across the entire functional network, False Discovery Rate (FDR) thresholding was applied to the final correlation values.

Results

Behavioral task acquisition and baseline performance

Thirty-two participants completed the study, which included an initial fMRI session (Day 1; Figure 1A) and a behavioral session outside the MRI scanner (Day 2; Figure 1B). The fMRI session was dedicated to acquiring rs-fMRI data, followed by an in-scanner cued hand-movement localizer task in which participants executed bimanual finger movements while wearing the MRI-compatible data glove (Figure 1A). During the behavioral session, participants performed a *de novo* motor skill learning task (Figure 1B). They learned to control an on-screen cursor to reach specific targets by moving either their right or left fingers via the data glove (see Methods for details). Participants were randomly assigned to one of two groups based on the hand used during the initial training phase: right-hand training followed by left-hand transfer (RL group), or left-hand training followed by right-hand transfer (LR group) (Figure 1B).

We calculated the task performance per block during the training (initial hand) and the transfer (opposite hand) phases. Task performance, defined as the proportion of time the cursor remained on the target during a trial, was used as the primary behavioral measure. Across both groups, participants successfully acquired the novel hand-cursor mapping, showing significant improvement in performance throughout the training and transfer phases (Figure 2A). Individualized curve-fitting of the performance time series showed a gradual increase in performance prior to reaching a plateau, characteristic of typical motor learning curves [21] (Figure 2B).

To assess the initial task performance, we compared the average of the first eight blocks of the training phase and transfer phases. Two-sided, within-group paired t-test revealed a significant improvement in initial task performance between the training and transfer phases for both the RL ($t(15) = 3.70$, $p = 0.002$) and LR ($t(15) = 5.89$, $p < 0.001$) groups, indicating that both

groups successfully transferred their performance across effectors. However, two-sided independent *t*-tests showed no difference between the two groups during either the training phase ($t(30) = 0.15$, $p = 0.88$), nor during the transfer phase ($t(30) = 1.38$, $p = 0.17$). Furthermore, to determine whether the subsequent learning dynamics were different in the transfer phase compared to initial acquisition, we calculated the slope of the performance improvement using individualized exponential fits. This analysis revealed no significant difference in learning rates in the transfer phases between the RL and LR group ($t(30) = 0.30$, $p = 0.76$).

Intermanual transfer

To evaluate the magnitude and directionality of the intermanual transfer in the *de novo* motor learning task, we first quantified the transfer rate. This metric isolates the initial performance advantage observed immediately upon switching hands, calculated relative to the total change in performance achieved during the initial training phase (see Methods). An independent *t*-test revealed no difference in transfer rates between the LR and RL groups ($t(30) = 1.42$, $p = 0.16$). Similarly, comparing the exponential rate constants (slope parameters) derived from the individualized curve-fitting models yielded no significant group differences ($t(30) = 0.29$, $p = 0.76$). When transfer was summarized using individual-level metrics, we did not find significant evidence for a group difference between the RL and LR groups (Figure S1). We therefore conducted a complementary analysis of the full block-wise learning curves using linear mixed-effects modeling. This approach allowed us to test phase-specific group differences while accounting for repeated observations within participants.

Linear mixed-effects modeling of phase-specific asymmetry

Given the substantial inter-subject variability in learning curves (Figure 2B), we applied a linear mixed-effects (LME) model. This model allowed us to account for individual baseline differences while testing whether performance changes across blocks and phases differed between the LR and RL groups. Task performance served as the dependent variable, with Block, Group (RL vs. LR), and Phase (training vs. transfer) as fixed effects, alongside their interactions (Table 1).

The LME model revealed a significant effect main effect of Block ($\beta = 0.009$, $t(3,034) = 30.77$, $p < 0.001$), confirming that participants steadily improved their performance over time. Additionally, a significant main effect of Phase ($\beta = 0.174$, $t(3,034) = 15.42$, $p < 0.001$) confirmed a robust transfer of performance within each group upon switching hands. Confirming our previous initial task performance comparison, there was no difference in task performance between the RL and LR groups ($\beta = -0.009$, $t(35.28) = -0.23$, $p = 0.814$).

Crucially, the LME allowed us to test for specific interactions between these factors. A significant Block × Phase interaction ($\beta = -0.003$, $t(3,034) = -7.75$, $p < 0.001$) demonstrated that the dynamic slope of performance improvement was dependent on the learning stage, with participants exhibiting faster improvements during the initial training phase compared to the following transfer phase.

Furthermore, once the model controlled for individual variance, a significant Group × Phase interaction emerged ($\beta = -0.066$, $t(3,034) = -4.14$, $p < 0.001$). The specific improvement in baseline execution from the training phase to the transfer phase was significantly larger for the LR group than the RL group. Ultimately, these LME results indicate that while both groups showed

similar overall trajectories of performance growth, the specific intermanual transfer of initial performance is highly asymmetric, favoring the left-to-right-hand transition.

Influence of plateau on transfer dynamics

Previous research suggests that the magnitude of intermanual transfer can be influenced by the extent of training, particularly whether practice continues after reaching an observable performance plateau [18]. To determine if attaining this stable execution ceiling influenced transfer dynamics in our task, we conducted a complementary analysis. Participants within each group were divided based on whether they successfully reached a performance plateau during the initial training phase. Plateau achievement was mathematically defined based on the asymptote of each participant's individualized exponential curve fit. Based on this criterion, 6 out of 16 participants in the LR group and 7 out of 16 participants in the RL group successfully reached a performance plateau prior to the end of the initial training phase. For these individuals, the stable execution ceiling was attained, on average, at block 31.6 (*SD* = ±15.2) for the LR group and block 35.2 (*SD* = ±8.0) for the RL group.

To assess the impact of reaching this execution ceiling, we compared the normalized transfer rate within each group. Independent samples *t*-tests revealed no significant differences in the transfer rate between those who reached a plateau and those who did not, neither within the LR group ($t(14) = 1.19$, $p = 0.25$) nor within the RL group ($t(14) = 0.53$, $p = 0.60$).

Resting-state functional connectivity associated with intermanual transfer

Using data from the localizer on Day 1 (Figure 1A), we estimated a first-level GLM modeling three different movement conditions: the left-hand, right-hand and both-hands conditions. The resulting subject-level activity maps were entered in a second-level one-sample t-test to determine group-level activation maps. This step provided a functional baseline to define regions of interest (ROIs) for the subsequent functional connectivity analysis. A conjunction analysis between activity maps for left-hand and right-hand movements identified 15 ROIs, including the inferior parietal lobule (IPL), intraparietal sulcus (IPS), cerebellum lobule VI and VIII (CB6 and CB8), Putamen, PMd and the ventral premotor area (PMv) in each hemisphere, and SMA (Figure 3). The peak coordinates extracted from these regions (intersected with atlases) were subsequently used as the anatomical nodes for predicting the observed behavioral asymmetry (Table S1).

To identify the functional pathways associated with intermanual transfer, the Fisher z-transformed resting-state connectivity of all 105 unique region-to-region edges (Figure S1) was correlated with the normalized intermanual transfer rate across subjects (Figure S2). It is notable that the original transfer rate should be normalized within each group to isolate individual variability and correct for learning order (Left-to-Right vs. Right-to-Left), thus effectively removing the main group effect and allowing for within-group comparisons.

To control for multiple comparisons across the 15-node network, FDR correction was applied. As shown in Figure 4, we found that the resting-state connectivity between the SMA and the left IPS showed significant correlation with the behavioral transfer rate ($r = 0.61$, $p_{FDR} = 0.01$, *95% CI* [*0.33, 0.79*]). Additionally, the SMA and right PMd connection was associated with better transfer rate ($r = 0.55$, $p_{FDR} = 0.021$, *95% CI* [*0.25, 0.75*]), as well as the SMA and left IPL ($r = 0.56$, $p_{FDR} = 0.021$, 95% CI $[0.26, 0.76]$).

Alongside the SMA, the left IPS-IPL exhibited the highest localized intra-hemispheric correlation with the transfer rate ($r = 0.63$, $p_{FDR} = 0.010$, 95% CI $[0.36, 0.80]$) and the left IPS also showed strong inter-hemispheric coupling with the right PMd ($r = 0.58$, $p_{FDR} = 0.020$, 95% CI $[0.28, 0.76]$) and left PMd ($r = 0.53$, $p_{FDR} = 0.026$, 95% CI $[0.22, 0.74]$). We also found a significant connection between the left IPS and left CB8 associated with higher transfer rate ($r = 0.54$, $p_{FDR} = 0.026$, 95% CI $[0.23, 0.74]$).

Discussion

In this study, we designed a *de novo* motor skill learning experiment that requires the acquisition of an entirely new visuomotor mapping to understand the neural mechanisms of intermanual transfer. Our behavioral results demonstrate that while both the RL and LR groups showed successful intermanual transfer following the initial training phase, the magnitude of the transfer was asymmetric, with larger performance gains when transferring from the left hand to the right hand than in the opposite direction. The behavioral experiment showed no significant difference between the two groups in the initial training phase, which is consistent with previous research that cognitive mappings are symmetrical in both hands during the early learning phase [5]. It suggests that in the early stages of learning a new motor skill, strategies are formed to learn common cognitive mappings regardless of hand, suggesting that both hands can begin learning a new skill in a similar way during the initial learning phase. However, as shown by the LME model results, the group that first learned with the non-dominant hand (left hand) in the training phase showed higher initial performance when transferring to the dominant hand (right hand) than the other group (Figure 2). We propose that this transfer asymmetry reflects an interplay between coordinate-dependent representations, hemispheric lateralization, and intermanual differences in motor execution. During *de novo* skill learning, individuals may form effector-independent representations that exist in extrinsic, world-centered reference frames, rather than relying solely on effector-specific intrinsic coordinates [17]. Because these extrinsic representations are inherently effector-independent, spatial mapping acquired by the non-dominant hand can be effectively utilized by the dominant hand [17]. Previous research suggests that the encoding of such effector-independent motor memories, driven by implicitly evolving mechanisms, is predominantly lateralized to the left hemisphere, involving regions such as the posterior parietal cortex, regardless of the hand used during initial training [18]. Since the left hemisphere directly controls the dominant right hand, the right hand may possess an anatomical advantage in accessing this shared motor memory during the transfer phase [18]. Alternatively, the behavioral manifestation of the transferred mapping likely depends on the inherent execution capabilities of each hand. According to the dynamic-dominance hypothesis, the dominant arm is specialized for controlling hand dynamics and trajectory formation [40]. Consequently, the dominant right hand might execute the transferred spatial representations more proficiently than the left hand. Together, these mechanisms suggest that the post-learning transfer phase is heavily dependent on the sensorimotor loop, which becomes increasingly engaged as learning progresses [24].

In addition, this study sought to interpret how individual differences in *de novo* motor learning skill transfer relate to intrinsic neural substrates identified via rs-fMRI. At the neural level, we found an interconnected pre-learning resting-state network, including the left IPS, PMd, IPL,

CB8, SMA and right PMd, that correlates with individual transfer rates. This sensorimotor network is centered on the left IPS, serving as a functional hub that links the whole network fronto-parietal and cerebellar systems. This finding likely captures the fact that the PPC, and more specifically the IPS, is involved in sensorimotor processes during the learning of a complex new set of rules, like manipulating a 2D cursor using distinct joint angles or using complex tools [26, 41]. The prominent role of the IPS in this network aligns with its established function in mapping extrinsic information into effector-independent motor representations [17, 42]. The significant coupling between the left IPS and SMA may support the translation of effector-independent visuomotor representations into coordinated, bilateral motor movements, consistent with the SMA's established role in intermanual coordination and motor sequence selection [13, 43]. These results provide an account of intermanual transfer: individual capacity for skill generalization is not determined by a single isolated region, but by the baseline functional integrity of the sensorimotor network that links spatial planning (IPS, IPL) with coordinated motor execution (SMA, PMd, CB8).

Nevertheless, the present study presents several limitations. First, our metric of transfer rate was calculated based on early or late phase averages to account for baseline individual differences. While such block-averaged definitions are standard, they may obscure fine-grained, trial-by-trial temporal dynamics. However, we mitigated this limitation by implementing linear mixed-effects (LME) modeling and exponential curve fitting to capture individualized plateau attainments and block-by-block performance trajectories, ensuring our transfer estimates were not disproportionately skewed by maximum execution capacities. Nevertheless, the transfer rate is calculated on the basis that each learning step is common across all participants and is still considered to be a robust way of defining the transfer rate. Second, while our overall sample size is comparable to those of typical motor learning studies, between-group design inherently limits our statistical power. Future studies would benefit from a larger sample size to robustly replicate the observed asymmetric transfer dynamics and to further explore how interactions within large-scale neural networks contribute to intermanual transfer.

Also, while the goal was to ensure that *de novo* skill learning was sufficiently learned, the experiments were more cognitively demanding than those utilized in previous studies. The task required constant hand movement while wearing a data glove, making it difficult to determine saturation of learning. The substantial inter-subject variability observed in our behavioral data, particularly regarding when participants reached a performance plateau, warrants further consideration. Why might performance ceiling fail to show significant influence on transfer dynamics in a *de novo* task, despite its reported effects in motor adaptation? [18] This discrepancy likely stems from the differing neural demands of acquiring a novel skill. Early *de novo* training is characterized by a high degree of cognitive exploration and reliance on broad, distributed cortical-subcortical networks to establish a totally new sensorimotor mapping [21]. It is within this early, dynamic window of rapid performance improvement that the generalized neural representation is constructed. As performance approaches a plateau, the underlying learning strategy may shift from global exploration toward localized, effector-specific exploitation, primarily fine-tuning the execution parameters of the active hand. Consequently, it is possible that the foundational neural representations required for intermanual transfer are sufficiently established prior to this late-stage fine-tuning. Furthermore, the highly variable attainment of a performance ceiling in our study might reflect the high cognitive demands of the task itself, such as the requirement for continuous,

isolated finger movements while wearing a data glove. To further elucidate these dynamics, a paradigm similar to Kumar et al., using a de *novo* motor learning task would be appreciated [18].

Finally, future research should systematically validate the causal relationship between specific brain regions and learning transfer using non-invasive brain stimulation such as transcranial magnetic stimulation (TMS) combined with fMRI [44]. TMS has the advantage of causally inferring the functional role of specific brain regions and, when combined with fMRI, can be utilized as a powerful tool to assess functional connectivity at the network level. The results of sthis study are correlational and do not establish causality. Previous studies have also found that stimulating the left posterior parietal cortex using transcranial direct current stimulation impaired learning, potentially due to perturbation of the encoding of hand-independent memory [18]. This study thus identified the parietal cortex as a key neural substrate for encoding effector-independent motor memory.

Conclusion

The present study reveals that functional interactions within the sensorimotor network significantly correlated with individual capacity for intermanual transfer in *de novo* motor skill learning. Behaviorally, we observed a directional asymmetry, wherein transfer from the left hand to the right hand is more efficient than the reverse. These findings may provide important insights for designing targeted rehabilitation strategies for patients with unilateral hand deficits by enabling individualized training of the less-affected hand to facilitate motor recovery and skill transfer to the affected hand.

Abbreviations

AFNI: Analysis of Functional NeuroImages; APQC: afni_proc.py quality control; BOLD: blood oxygen level–dependent; CS: central sulcus; DoF: degree of freedom; EPI: echo-planar imaging; FA: flip angle; FOV: field of view; fMRI: functional magnetic resonance imaging; FWHM: full width at half maximum; GE-EPI: gradient-echo echo-planar imaging; GLM: general linear model; IPS: inferior parietal sulcus; IRB: Institutional Review Board; LME: linear mixed-effects (model); LR: Left-to-Right group; M1: primary motor cortex; MNI: Montreal Neurological Institute; MPRAGE: magnetization-prepared rapid gradient echo; MRI: magnetic resonance imaging; NAS: Network Attached Storage; PCA: principal component analysis; PMd: dorsal premotor cortex; PPC: posterior parietal cortex; RL: Right-to-Left group; ROI: region of interest; rs-fMRI: resting-state functional magnetic resonance imaging; SEM: standard error of the mean; SMA: supplementary motor area; SNR: signal-to-noise ratio; STS: superior temporal sulcus; TE: echo time; TMS: transcranial magnetic stimulation; TR: repetition time; ; vmPFC: ventromedial prefrontal cortex.

Author contributions

S.K. conceived the idea presented in the study and designed the experiment. Y.K. and S.E. performed the experiment. Y.K, A.C., and S.E. performed formal analysis; Y.K,, A.C., and S.K. wrote the manuscript. S.K. supervised the entire procedure of the study.

Acknowledgements

Neuroimaging was performed at the Center for Neuroscience Imaging Research located at Sungkyunkwan University, supported by the Institute for Basic Science. This work was supported by the National Research Foundation of Korea (NRF-2021R1A2C2011648, RS-2024-00356694), Hanyang University and Korea Basic Science Institute (KBSI) (HY-202400000003862), Yangyoung Foundation.

Data availability

All MRI data used in this study are archived in the Hanyang University Network Attached Storage (NAS). Upon reasonable request, the corresponding author can provide all the dataset and code related to this study.

Declarations

Ethics approved and consent to participate

The Institutional Review Board (IRB) of Sungkyunkwan University, Suwon, South Korea approved all procedures related to the study following safety protocols (IRB No. 2018-05-003-032). We performed all the research methods in accordance with the Declaration of Helsinki.

Consent for publication

Prior to the first experiment, all participants provided written informed consent and received monetary compensation for their participation.

Competing interests

The authors declare no competing interests.

References

1. Krakauer JW, Mazzoni P, Ghazizadeh A, Ravindran R, Shadmehr R. Generalization of motor learning depends on the history of prior action. *PLoS Biol*. 2006;4(10):e316. doi:10.1371/journal.pbio.0040316.
2. Perez MA, Tanaka S, Wise SP, Sadato N, Tanabe HC, Willingham DT, et al. Neural substrates of intermanual transfer of a newly acquired motor skill. *Curr Biol*. 2007;17(21):1896-1902.
3. Kirsch W, Hoffmann J. Asymmetrical intermanual transfer of learning in a sensorimotor task. *Exp Brain Res*. 2010;202(4):927-934. doi:10.1007/s00221-010-2184-8.
4. Schulze K, Lüders E, Jäncke L. Intermanual transfer in a simple motor task. *Cortex*. 2002;38(5):805-815. doi:10.1016/S0010-9452(08)70047-9.
5. Yadav G, Mutha PK. Symmetric interlimb transfer of newly acquired skilled movements. *J Neurophysiol*. 2020;124(5):1364-1376. doi:10.1152/jn.00777.2019.
6. Wang Y, Zhao J, Inada H, Négyesi J, Nagatomi R. Impact of handedness on interlimb transfer depending on the task complexity combined with motor and cognitive skills. *Neurosci Lett*. 2022;785:136775. doi:10.1016/j.neulet.2022.136775.
7. Nozaki D, Kurtzer I, Scott SH. Limited transfer of learning between unimanual and bimanual skills within the same limb. *Nat Neurosci*. 2006;9:1364-1366.
8. Yokoi A, Bai W, Diedrichsen J. Restricted transfer of learning between unimanual and bimanual finger sequences. *J Neurophysiol*. 2017;117(3):1043-1051. doi:10.1152/jn.00387.2016.
9. Gooijers J, Swinnen SP. Interactions between brain structure and behavior: the corpus callosum and bimanual coordination. *Neurosci Biobehav Rev*. 2014;43:1-19. doi:10.1016/j.neubiorev.2014.03.008.
10. Anguera JA, Russell CA, Noll DC, Seidler RD. Neural correlates associated with intermanual transfer of sensorimotor adaptation. *Brain Res*. 2007;1185:136-151. doi:10.1016/j.brainres.2007.09.088.
11. Seidler RD. Neural correlates of motor learning, transfer of learning, and learning to learn. *Exerc Sport Sci Rev*. 2010;38(1):3. doi:10.1097/JES.0b013e3181c5cce7.
12. Swinnen SP. Intermanual coordination: from behavioural principles to neural-network interactions. *Nat Rev Neurosci*. 2002;3(5):348-359. doi:10.1038/nrn807.
13. Perez MA, Tanaka S, Wise SP, Willingham DT, Cohen LG. Time-specific contribution of the supplementary motor area to intermanual transfer of procedural knowledge. *J Neurosci*. 2008;28(39):9664-9669.
14. Paparella G, De Riggi M, Cannavacciuolo A, Colella D, Costa D, Birreci D, et al. Relationship between the interlimb transfer of a visuomotor learning task and interhemispheric inhibition in healthy humans. *Cereb Cortex*. 2023;33(12):7335-7346. doi:10.1093/cercor/bhad042.
15. Gerraty RT, Davidow JY, Wimmer GE, Kahn I, Shohamy D. Transfer of learning relates to intrinsic connectivity between hippocampus, ventromedial prefrontal cortex, and large-scale networks. *J Neurosci*. 2014;34(34):11297-11303. doi:10.1523/JNEUROSCI.0185-14.2014.
16. Dirren E, Bourgeois A, Klug J, Kleinschmidt A, van Assche M, Carrera E. The neural correlates of intermanual transfer. *Neuroimage*. 2021;245:118657. doi:10.1016/j.neuroimage.2021.118657.

17. Wiestler T, Waters-Metenier S, Diedrichsen J. Effector-independent motor sequence representations exist in extrinsic and intrinsic reference frames. *J Neurosci*. 2014;34(14):5054-5064. doi:10.1523/JNEUROSCI.5363-13.2014.
18. Kumar A, Panthi G, Divakar R, Mutha PK. Mechanistic determinants of effector-independent motor memory encoding. *Proc Natl Acad Sci U S A*. 2020;117(29):17338-17347. doi:10.1073/pnas.2001179117.
19. Mazzoni P, Krakauer J. An implicit plan overrides an explicit strategy during visuomotor adaptation. *J Neurosci*. 2006; 26:3642-3645.
20. Shadmehr R, Smith M, Krakauer J. Error correction, sensory prediction, and adaptation in motor control. *Annu Rev Neurosci*. 2010; 33, 89-108.
21. Krakauer J, Hadjiosif A, Xu J, Wong A, Haith A. Motor learning. *Compr Physiol*. 2019;9:613-663. doi:10.1002/cphy.c170043.
22. Telgen S, Parvin D, Diedrichsen J. Mirror reversal and visual rotation are learned and consolidated via separate mechanisms: recalibrating or learning de novo? *J Neurosci*. 2014; 34:13768-13779.
23. Sternad D. It's not (only) the mean that matters: variability, noise and exploration in skill learning. *Curr Opin Behav Sci*. 2018; 20:183-195.
24. Choi Y, Shin EY, Kim S. Spatiotemporal dissociation of fMRI activity in the caudate nucleus underlies human de novo motor skill learning. *Proc Natl Acad Sci U S A*. 2020;117(38):23886-23897. doi:10.1073/pnas.2003963117.
25. Liu X, Scheidt RA. Contributions of online visual feedback to the learning and generalization of novel finger coordination patterns. *J Neurophysiol*. 2008;99(5):2546-2557. doi:10.1152/jn.01044.2007.
26. Ossmy O, Mukamel R. Neural network underlying intermanual transfer of motor experience. *Cell Rep*. 2016;14(10):2288-2294.
27. Takeda Y, Takano K, Nakamura T. Network coupling during motor learning and transfer. *iScience*. 2026.
28. Bassett DS, Yang M, Wymbs NF, Grafton ST. Learning-induced autonomy of sensorimotor systems. *Nat Neurosci*. 2015;18(5):744-751.
29. Mattar MG, Wymbs NF, Bock AS, Aguirre GK, Grafton ST, Bassett DS. Predicting future learning from baseline network architecture. *NeuroImage*. 2018;172:107-117.
30. Manuel AL, Guggisberg AG, Thézé R, Turri F, Schnider A. Resting-state connectivity predicts visuo-motor skill learning. *NeuroImage*. 2018;176:446-453.
31. Carroll TJ, Herbert RD, Munn J, Lee M, Gandevia SC. Contralateral effects of unilateral strength training: evidence and possible mechanisms. *J Appl Physiol*. 2006;101(5):1514-1522.
32. Lee M, Carroll TJ. Cross education: possible mechanisms for the contralateral effects of unilateral resistance training. *Sports Med*. 2007;37(1):1-14.
33. Manca A, Hortobágyi T, Carroll TJ, Enoka RM, Farthing JP, Gandevia SC, et al. Contralateral effects of unilateral strength and skill training: modified Delphi consensus to establish key aspects of cross-education. *Sports Med*. 2021;51(1):11-20.
34. Oldfield RC. The assessment and analysis of handedness: the Edinburgh inventory. *Neuropsychologia*. 1971;9(1):97-113. doi:10.1016/0028-3932(71)90067-4.

35. Cox RW. AFNI: software for analysis and visualization of functional magnetic resonance neuroimages. *Comput Biomed Res*. 1996;29(3):162-173.
36. Cox RW, Hyde JS. Software tools for analysis and visualization of fMRI data. *NMR Biomed*. 1997;10(4-5):171-178.
37. Reynolds RC, Glen DR, Chen G, Saad ZS, Cox RW, Taylor PA. Processing, evaluating, and understanding fMRI data with afni_proc.py. *Imaging Neurosci*. 2024;29:1-?.
38. Fan L, Li H, Zhuo J, Zhang Y, Wang J, Chen L, Yang Z, Chu C, Xie S, Laird AR, Fox PT, Eickhoff SB, Yu C, Jiang T. The Human Brainnetome Atlas: A New Brain Atlas Based on Connectional Architecture. *Cereb Cortex*. 2016 Aug;26(8):3508-26. doi: 10.1093/cercor/bhw157.
39. Diedrichsen J, Balsters JH, Flavell J, Cussans E, Ramnani N. A probabilistic atlas of the human cerebellum. *Neuroimage*. 2009.
40. Sainburg RL. Evidence for a dynamic-dominance hypothesis of handedness. *Exp Brain Res*, 2002; 142(2): 241-258.
41. Creem-Regehr SH. Sensory-motor and cognitive functions of the human posterior parietal cortex involved in manual actions. *Neurobiol Learn Mem*. 2009;91(2):166-171.
42. Mutha PK, Sainburg RL, Haaland KY. Left parietal regions are critical for adaptive visuomotor control. *J Neurosci*. 2011;31(18):6972-6981.
43. Welniarz Q, Gallea C, Lamy JC, et al. The supplementary motor area modulates interhemispheric interactions during movement preparation. *Hum Brain Mapp*. 2019;40:2125-2142. doi:10.1002/hbm.24512.
44. Haber SN, Calzavara R. The cortico-basal ganglia integrative network: the role of the thalamus. *Brain Res Bull*. 2009;78(2-3):69-74.
45. Bosch-Bouju C, Hyland BI, Parr-Brownlie LC. Motor thalamus integration of cortical, cerebellar and basal ganglia information: implications for normal and parkinsonian conditions. *Front Comput Neurosci*. 2013;7:163. doi:10.3389/fncom.2013.00163.

Figures

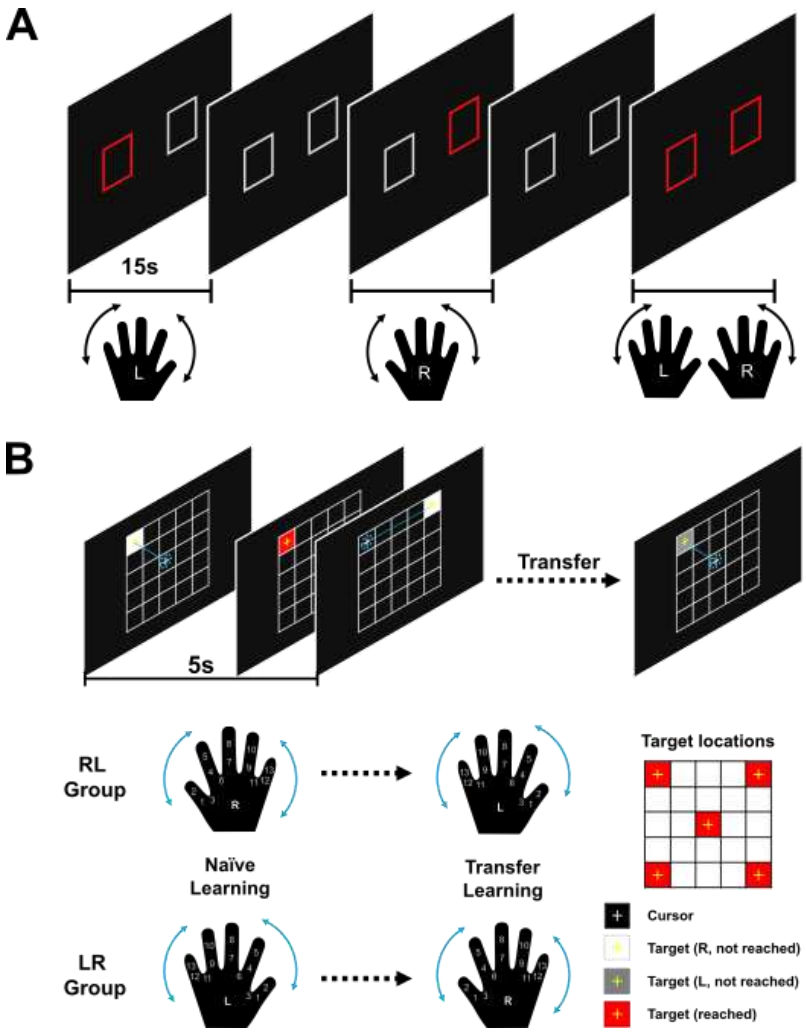


Figure 1. Experimental design

(A) Cued motor movement task for the fMRI experiment. During the first day, participants completed a localizer scan to isolate brain regions involved in hand movements inside the MRI scanner while wearing MR-compatible gloves that recorded finger joint movements in real time. During each trial, two grey squares were presented on the screen. The appearance of a red square indicated which hand the participant had to move based on its position on the screen (the left square for the left hand, the right square for the left hand, or both squares for both hands). Each trial lasted for 15 seconds, followed by a 15-second rest period. (B) Behavioral experiment. During the second day, participants performed a *de novo* motor learning task outside the MRI scanner. Participants first learned to move a crosshair cursor on the screen to reach targets located in the center and at the four corners of a 5 x 5 grid, using finger movements of either their right or left hand (naïve learning). Next, they performed the same task using their contralateral hand (transfer learning). Participants in the RL group used their right hand for naïve learning, while participants in the LR group used their left hand.

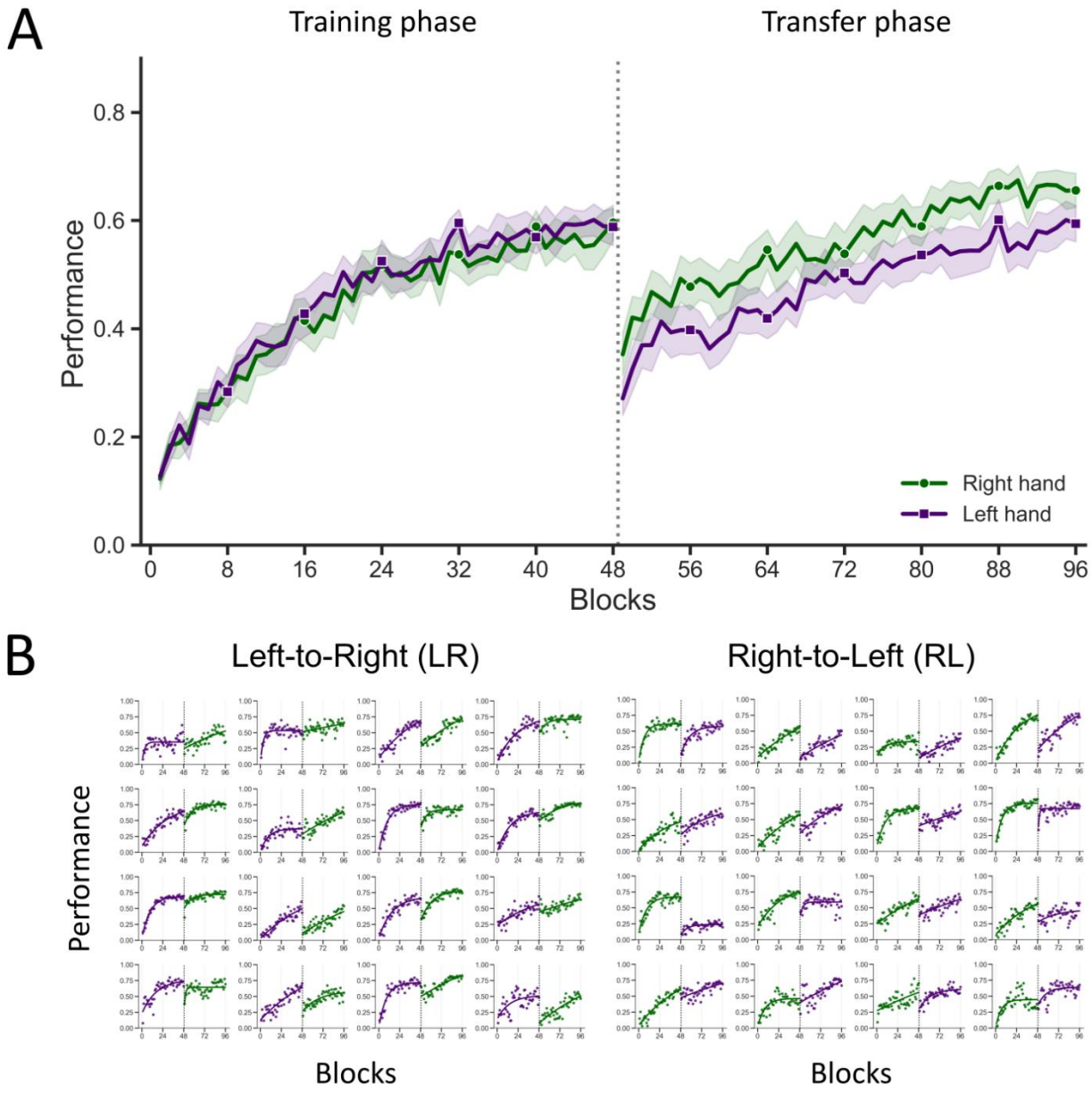


Figure 2. **Performance dynamics during intermanual transfer training of *de novo* task** (A) Average group performance. Solid lines represent the mean performance per block for the Left-to-Right (LR) and Right-to-Left (RL) groups during the training (blocks 1–48) and transfer (blocks 49–96) phases. Shaded regions indicate the standard error of the mean (SEM). The vertical dotted line marks the hand-switch transition between training and transfer. (B) Individual participant performance. Each panel represents a single participant behavioral data. Scatter points represent single-subject performance at each block, overlaid with lines indicating the fitted exponential growth model (see Methods for details). Across both panels, color denotes the active hand (purple = left hand; green = right hand).

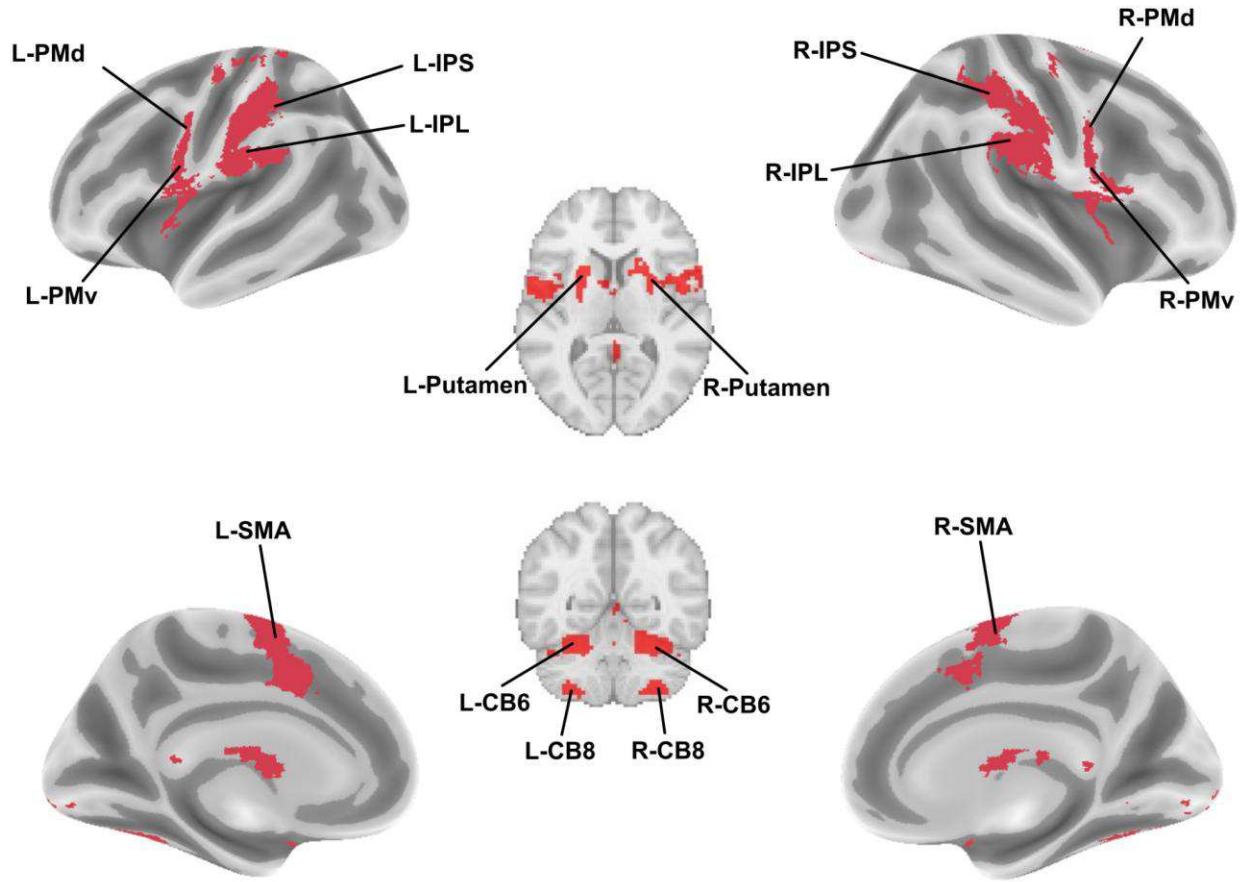


Figure 3. **ROIs within the sensorimotor network identified in the localizer session**
ROIs selected for the functional connectivity analysis. Left (L-) and right (R-) hemispheres are indicated. Specific brain regions highlighted in red overlays are labeled with abbreviations: PMd (Dorsal Premotor cortex); PMv (Ventral Premotor cortex); IPS (Intraparietal Sulcus); IPL (Inferior Parietal Lobule); Putamen; SMA (Supplementary Motor Area); CB6 (Cerebellar Lobule 6); and CB8 (Cerebellar Lobule 8). The ROIs are displayed on standardized brain templates from lateral (top rows), medial (bottom-left and bottom-right), subcortical axial (center), and inferior/basal (bottom-center) views.

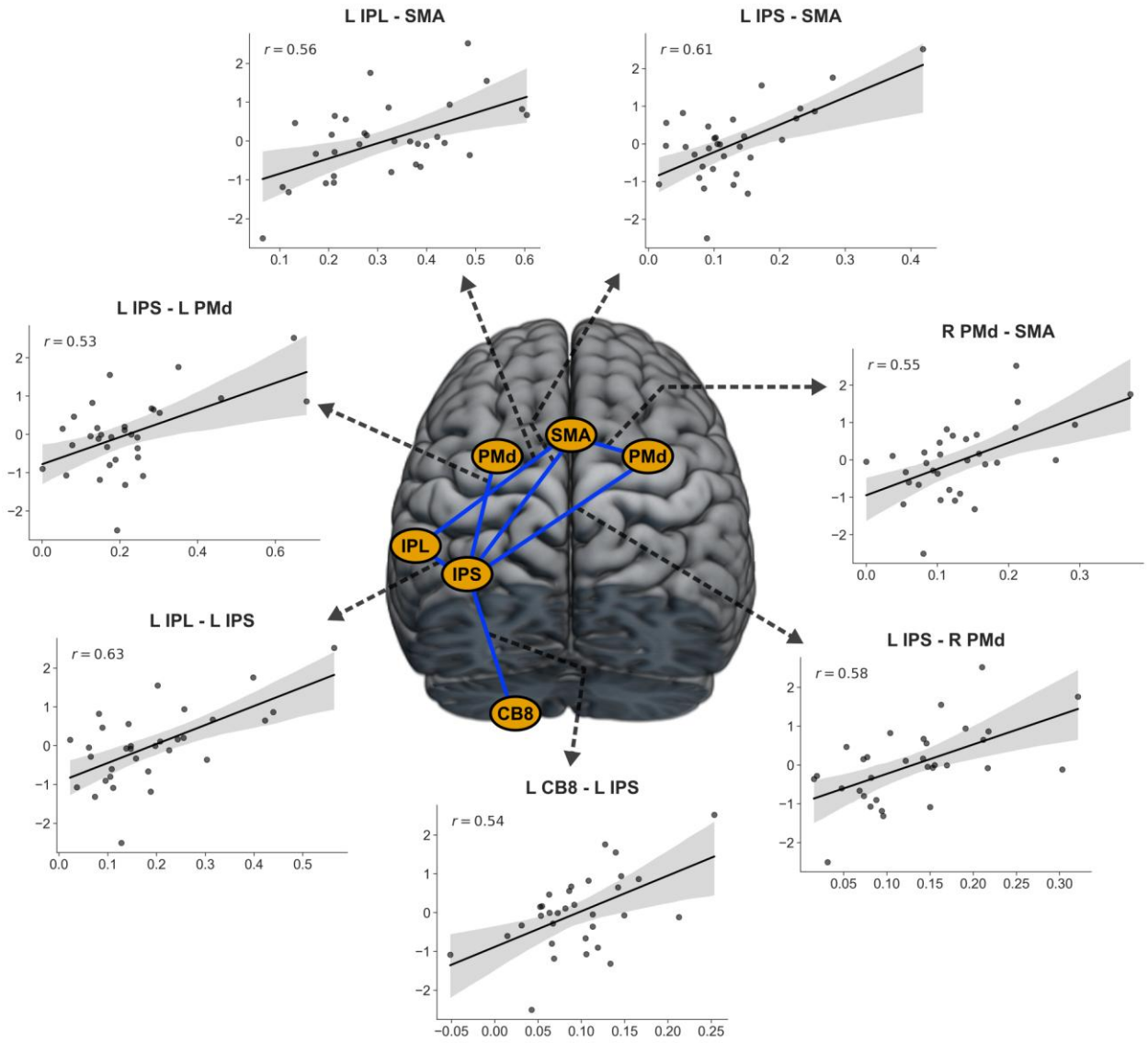


Figure 4. Functional connections within the sensorimotor network associated with the normalized transfer rate.

Blue lines indicate the significant functional connections correlated with normalized transfer rates after FDR correction (q(FDR) < 0.05). Individual scatter plots demonstrate the significant positive correlations between the Fisher *z*-transformed functional connectivity strength of each neural connection (x-axis) and the normalized transfer rate (y-axis). Each plot includes individual subject data points (gray dots), a solid black linear regression line, and shaded regions representing the 95% confidence intervals. Pearson correlation coefficients (*r*) are reported in the top-left corner of each panel. Abbreviations: L, Left; R, Right; SMA, Supplementary Motor Area; PMd, Dorsal Premotor Cortex; IPL, Inferior Parietal Lobule; IPS, Intraparietal Sulcus; CB8, Cerebellar Lobule 8.

Table 1: Summary of the linear mixed-effects model analysis for the performance across groups

Fixed effects coefficients	Estimate	Standard error	T-value	P value	Degree of freedom (DoF)
Intercept	0.2476	0.0268	9.239	< 0.001	35.28
Block	0.0087	0.0003	30.777	< 0.001	3,034
Group	-0.0089	0.0379	-0.237	0.814	35.28
Phase	0.1741	0.01128	15.429	< 0.001	3,034
Block x Group	-0.0004	0.0004	-0.888	0.374	3,034
Block x Phase	-0.0031	-0.0004	-7.754	< 0.001	3,034
Group x Phase	-0.0662	0.0159	-4.149	< 0.001	3,034
Block x Group x Phase	0.0002	0.0005	0.433	0.665	3,034

Supplementary Figures

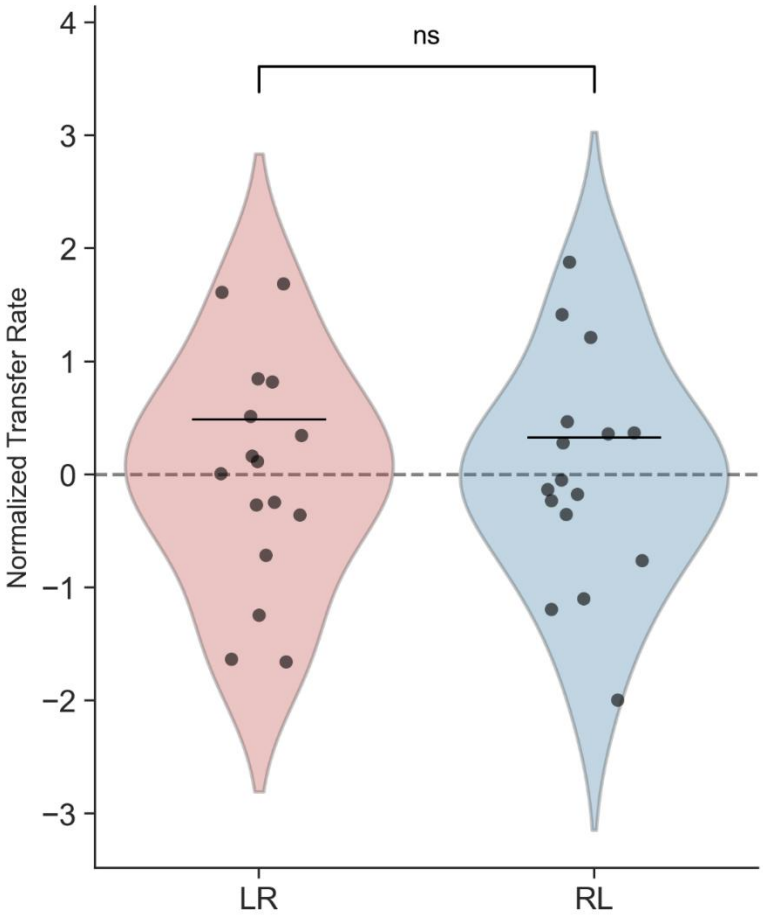


Figure S1. Distribution of intermanual transfer rate.
Violin plots illustrate the normalized transfer rate for the Left-to-Right (LR) and Right-to-Left (RL) groups. Individual participant data points are overlaid as semi-transparent black circles, highlighting the high degree of inter-subject variability within both groups. The black horizontal lines denote the mean transfer rate for each respective group. The dashed gray line at $y = 0$ represents a theoretical baseline of zero transfer, where positive values indicate a facilitation of initial performance upon switching hands, and negative values indicate a relative performance decrement (ns = not significant; $p > 0.05$).

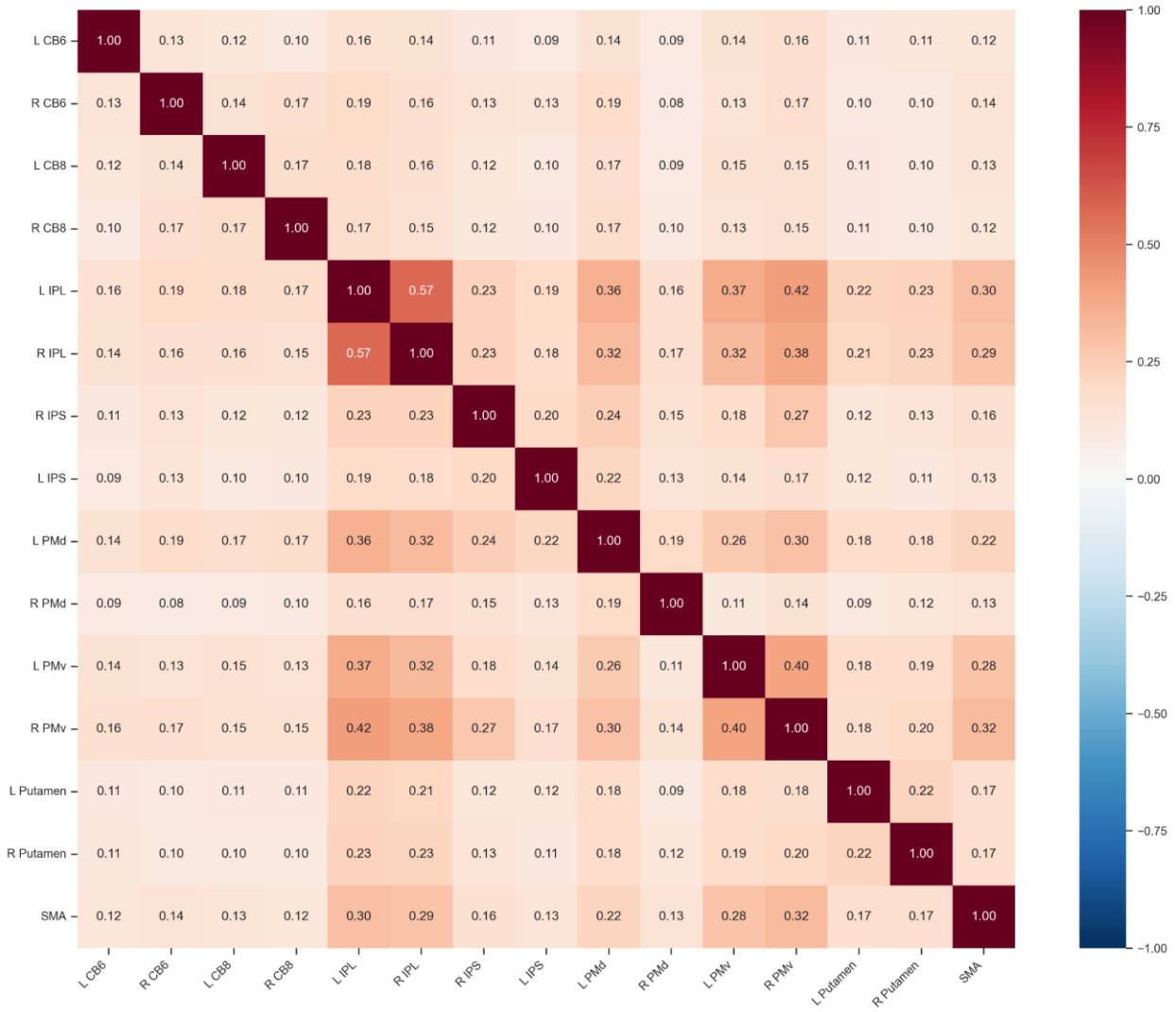


Figure S2. Group average resting-state functional connectivity within the sensorimotor network

The heatmap displays the mean functional connectivity between 15 pre-defined regions of interest (ROIs) across all participants. Individual subject correlation matrices were first Fisher *z*-transformed, averaged across the group, and subsequently back-transformed to Pearson correlation coefficients (*r*) for visualization. Numerical values within each cell represent the mean *r*-value for that specific neural connection. The color gradient indicates the strength of the connectivity, with darker red colors representing stronger positive correlations. Abbreviations: L, Left; R, Right; CB6, Cerebellar Lobule 6; CB8, Cerebellar Lobule 8; IPL, Inferior Parietal Lobule; IPS, Intraparietal Sulcus; PMd, Dorsal Premotor Cortex; PMv, Ventral Premotor Cortex; SMA, Supplementary Motor Area.

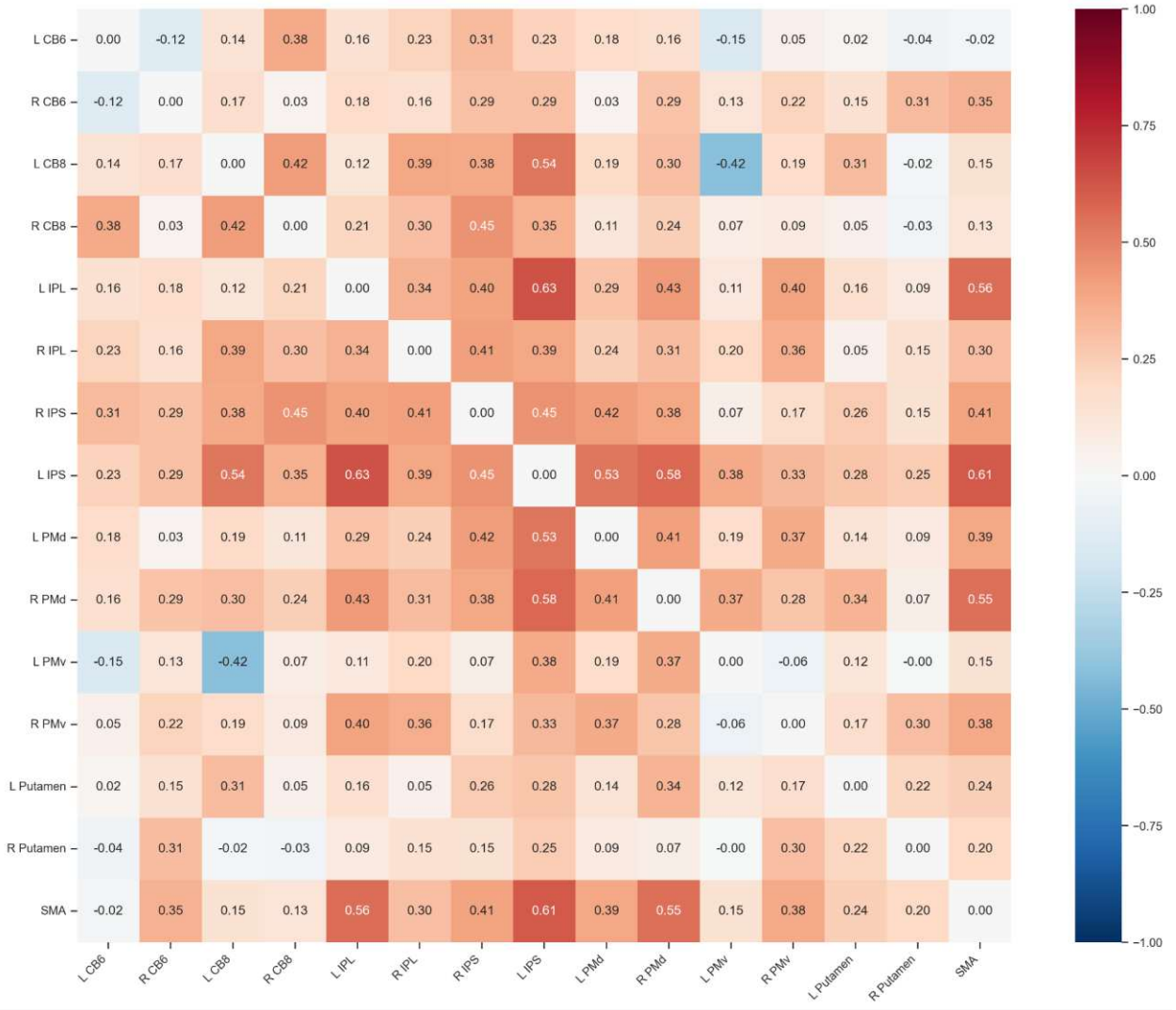


Figure S3. Brain-behavior correlation matrix for intermanual transfer.
Brain-behavior relationship matrix displaying the correlation coefficients (*r*) between the intrinsic resting-state functional connectivity of 15 seed regions and the normalized intermanual transfer rate across participants. Color intensity reflects the strength and direction of the correlation, with dark red indicating a strong positive association between regional coupling and behavioral transfer to the untrained hand. Widespread significant correlations are observed within a targeted fronto-parietal network, highlighting the Supplementary Motor Area (SMA), dorsal premotor cortex (PMd), and the parietal cortex (IPS/IPL) as pre-learning indicators associated with intermanual transfer in de *novo* motor skill.

871 **Table S1. Peak activation coordinates for the ROIs**

	Peak (MNI)		
	X	*Y*	*Z*
L Intraparietal sulcus	−35	−36	45
R Intraparietal sulcus	37	−36	55
L Inferior parietal lobule	−48	−58	−46
R Inferior parietal lobule	51	−31	28
L Putamen	−27	−1	12
R Putamen	29	1	−6
L Cerebellum VI	−24	−59	−20
R Cerebellum VI	21	−55	−22
L Cerebellum VIII	−21	−58	−46
R Cerebellum VIII	19	−58	−46
L dorsal Premotor	−37	−12	64
R dorsal Premotor	35	−12	66
L ventral Premotor	−59	6	23
R ventral Premotor	59	6	31
SMA	−10	−7	72

872

Supplementary Files

This is a list of supplementary files associated with this preprint. Click to download.

- Supplementaryfile.docx